Towards a non-Invasive Monitoring System for Wind Turbine Blades

Conference Paper

Author(s):
Schärer, Nicolas; Polonelli, Tommaso; Deparday, Julien; Magno, Michele

Publication date:
2024

Permanent link:
https://doi.org/10.3929/ethz-b-000689876

Originally published in:
https://doi.org/10.1109/I2MTC60896.2024.10561240

Towards a non-Invasive Monitoring System for Wind Turbine Blades

Nicolas Schärer
D-ITET, ETH Zürich
Zürich, Switzerland
0009-0000-8055-8511

Tommaso Polonelli
D-ITET, ETH Zürich
Zürich, Switzerland
0000-0003-0405-3612

Julien Deparday
IET, OST
Rapperswil, Switzerland
0000-0001-8040-546X

Michele Magno
D-ITET, ETH Zürich
Zürich, Switzerland
0000-0003-0368-8923

***Abstract*—Wind power generation plays a crucial role in transitioning away from fossil fuel-dependent energy sources, contributing significantly to the mitigation of climate change. Therefore, it is advantageous to enhance the adoption of wind energy while improving turbine conversion efficiency. Monitoring wind flow and operational parameters of wind turbines is a fundamental prerequisite for optimizing broad coverage and electrical conversion efficiency. The aerodynamics of the rotating blades are of particular interest but are very challenging to measure due to the complexity of measurement system installations on operating wind turbines. This paper presents a flexible and modular system that enables real-time monitoring on the surface of wind turbine blades. Experimental results demonstrate the capability of extracting key aerodynamic parameters, such as Angle of Attack (AoA) and flow detachment, using an array of commercial low-power sensors, i.e., 10 absolute pressure sensors, 5 differential pressure sensors, and a MEMS vibrometer with a precision of 1° and a maximum power consumption below 50 mW.**

***Index Terms*—wind turbine, aerodynamic, MEMS, sensors, IoT**

I. Introduction

Today, wind energy is considered one of the most important resources to significantly alleviate CO2 emissions and help mitigate global warming [1]. Based on the recently agreed EU target, the electricity grid must be composed of at least 42% of renewable energy by 2030. Thus, a massive increase in wind turbine capacity and efficiency is required, with an expected growth in electricity generation from $204\,\mathrm{GW}$ in 2022 to more than $500\,\mathrm{GW}$ in 2030 [2]. To widely adopt wind energy as a power source, optimizing the design and operation efficiency of wind turbines while reducing negative environmental impacts and maintenance costs is essential [2]. It demands a deeper understanding of the blade aerodynamics [3], specifically for off-shore wind farms where installation and periodic maintenance costs require a high volume of generated electricity to be commercially viable. Wind turbines operate in a turbulent airflow, encountering strong wind speed changes over time, which can cause load fluctuations, reduced lifespan, and less effective aerodynamic control [4]. Investigating these interactions is crucial in unsteady aerodynamics. A better understanding of unsteady turbulent flows over airfoils, such as wind turbine blades, would enhance dynamic force estimation and allow more efficient and adaptive airfoil control models. For that purpose, experimental data are necessary including parameters like Angle of Attack (AoA) and flow detachment, which is characterized by a separation point at which the flow does not follow the airfoil shape anymore. The separation point moves from the trailing edge to the leading edge as the AoA increases and worsens the aerodynamic performance [4]. However, nowadays, there is a lack of available experimental data for such airfoils with controlled turbulent inflow to measure flow structures and surface pressure responses.

Wireless Sensor Networks (WSN) hold promise for monitoring wind turbine structures, driven by the global interest in the Internet of Things (IoT). Many wireless systems use low-power, compact Micro-ElectroMechanical Systems (MEMS) sensors, including inertial measurement units (IMU) and pressure sensors [5]. Most commercial MEMS sensors are miniaturized System on Chip (SoC) devices featuring analog-to-digital conversion, digital and analog programmable filters, and, in some cases, a machine learning core. These systems enable on-device measurements and data processing, leveraging low-power processors like microcontrollers (MCU), while on-device feature extraction reduces network load for low-power, long-term installations [6].

Currently, wireless sensors monitoring large structures, like wind turbines, typically employ a limited number of devices [5], [6]. Recent works, namely the Aerosense system [6]–[8], have proven the possibility of installing battery-supplied and self-sustaining wireless sensor nodes directly on the surface of wind turbine blades. Therefore, enabling long-term operative and structural monitoring analysis from an aerodynamic perspective. However, due to wind turbine substantial dimensions (usually $1\,\mathrm{m}$ to $6\,\mathrm{m}$ chord length along a span of $70\,\mathrm{m}$ for a $5\,\mathrm{MW}$ wind turbine), deploying a large array of low-power, relatively high-frequency MEMS sensors on a large airfoil remains challenging. Ideally, a trade-off between measurement accuracy and power consumption should be found for more robust and long-term blade monitoring, with the optimal sensor selection and spatial distribution.

This work proposes a study to investigate the optimal sensor selection and sparse position optimization among commercial MEMS sensors to detect the main aerodynamic parameters of a wind turbine blade. The commercial MEMS sensors are selected by comparing the power consumption against the

The experiments were performed within the French-Swiss project MISTERY funded by the French National Research Agency (ANR PRCI grant no. 266157) and the Swiss National Science Foundation (grant no. 200021L 21271). Moreover, we truly thank ST Microelectronics for supporting this work.

accuracy and dimensions, aiming to provide the lowest power consumption and the smallest form factor. All the selected elements must have a thickness below $5\,\mathrm{mm}$ and a power consumption under $100\,\mathrm{mW}$. Results from a 1:1 scale wind turbine blade are collected from an array of three different MEMS elements, 10 absolute pressure sensors, 5 differential pressure sensors, and a vibrometer. The heterogeneous set of selected sensors consistently demonstrates the possibility to infer the blade AoA and to detect the flow detachment with a precision of 1° with a dedicated measurement system featuring a total thickness below $5\,\mathrm{mm}$ and a total power consumption of $49\,\mathrm{mW}$. Reported results support the active and real-time monitoring of wind flow and wind turbine operational parameters for optimizing coverage and electrical conversion efficiency.

To summarize, the main scientific contributions of this paper are: *(i)* design and development of a modular sensor system for airflow monitoring on an airfoil/wind turbine blade *(ii)* dataset acquisition in a wind tunnel using a 1:1 turbine blade at different AoA *(iii)* preliminary analysis of AoA and flow separation using low-cost low power MEMS absolute and differential pressure sensors and a MEMS vibrometer.

II. Related Works

The field of non-invasive wind turbine aerodynamics monitoring has become a relevant topic in recent years [9]. Wind turbines are becoming larger and larger, with blade lengths reaching up to 80 meters, and wind farms are being built in remote locations. This means that predictive maintenance and real-time monitoring are essential to maximize the generated energy and minimize the operational costs [10]. While several works are already exploring Structural Health Monitoring (SHM) via WSN installation on the tower and inside the generator, e.g., the gear and bearings, the *in-loco* aerodynamic tracing is mostly unexplored. For the former, vibration-based sensors are used, such as [9] or [11], where a MEMS IMU is used to detect faults in mechanical components. These measurement systems can be supplied by the power main or with a rechargeable battery.

Regarding aerodynamic monitoring, the current State-of-the-Art (SoA) present in the literature is driven by the Aerosense system [5], a self-sustaining monitoring system based on multi MEMS sensors and SoC MCU. The Aerosense system features pressure and acoustic MEMS sensor arrays and an IMU coupled with edge computing and photovoltaic energy harvesting to achieve in-field precise and sustainable data collection [6]. In particular, it is suitable for installation on a wide range of wind turbine blades hosting a modular sensor unit with up to 40 barometers and 10 microphones, in addition to 5 differential pressure sensors [6]. The wireless communication is based on Bluetooth Low Energy 5.1 (BLE), which enables wireless communication on a low-energy System-on-Chip (SoC) CC2652P from Texas Instruments. Although the Aerosense system has been proven to run reliably on operating wind turbines [6], [12], so far, works published in the literature mainly focus on the sensor design in terms of electronic components and installation. Moreover, the ultra-low power sensors selected for the Aerosense prototype have shown limitations regarding the sensor accuracy [8], [12], requiring long and tedious calibration procedures to reach the required absolute accuracy of $10\,\mathrm{Pa}$ [7]. While the Aerosense system has been designed to measure the aerodynamic properties of a wind turbine blade section with a large number (50+) of sensors, the system has problems in large installations, such as wind farms or blade chords longer than $1\,\mathrm{m}$, due to the large number of sensors that needs to be handled and time-synchronized. Thus it can be further optimized for very low power and robust long-term measurements using fewer sensor tabs. It would then imply an optimal sensor selection and sparse sensor position optimization.

Therefore, this paper builds upon the Aerosense concept of a heterogeneous measurement system targeted to perform ablation studies and comparisons among low-cost and low-power MEMS sensors regarding position, type, quantity, and sensor fusion algorithms in a controlled environment, i.e., a wind tunnel, to create the optimal sensor configuration for aerodynamic monitoring.

III. Experimental Setup

This paper details experiments conducted in the Jules Verne wind tunnel located in Nantes, France. Notably, all reported results stem from precise measurements carried out within this large wind tunnel. Owned by the Scientific and Technical Center for Building (CSTB), a public entity, the Jules Verne wind tunnel serves as a distinguished platform for our research endeavors. The test section, measuring 6 m in width and 5 m in height, accommodates the airfoil with a $1.25\,\mathrm{m}$ chord and a span of $5\,\mathrm{m}$. The maximum height is $25\,\mathrm{cm}$ (20% of the chord). It occurs at 33% of the chord length from the leading edge. The shape of the airfoil corresponds to a 1:1 scale of the section at 80% of the span of an operating $2\,\mathrm{MW}$ wind turbine blade [13]. The wind speed can reach $60\,\mathrm{m\,s^{-1}}$, reproducing the field conditions at a 1:1 scale. The AoA is varied using two jacks located at the extremities of the blade to be able to sustain $2\,\mathrm{t}$ of generated aerodynamic force and maintain an angular precision below 1°. The blade's structure has different hatches to install the acquisition system and wires inside the blade. On the blade surface, to measure the pressure distribution, a total of 350 high-quality pressure taps are distributed on the blade, which are used as a reference for our low-power and low-cost surface measurement system.

The wind tunnel control room is located at approximately $10\,\mathrm{m}$ from the blade, with a dedicated wired connection to each measurement system deployed in this experiment. Moreover, to ensure perfect data alignment during post-processing analysis, a dedicated wire distributes a $1\,\mathrm{Hz}$ TTL signal to all the boards for precise time synchronization.

A total of 18 tests were conducted, each consisting of two-minute acquisitions at a constant wind speed of $40\,\mathrm{m\,s^{-1}}$ with the blade setup in Figure 1 and Figure 3. Each acquisition has a varying AoA, from -10° to 28°, as described in Figure 1.

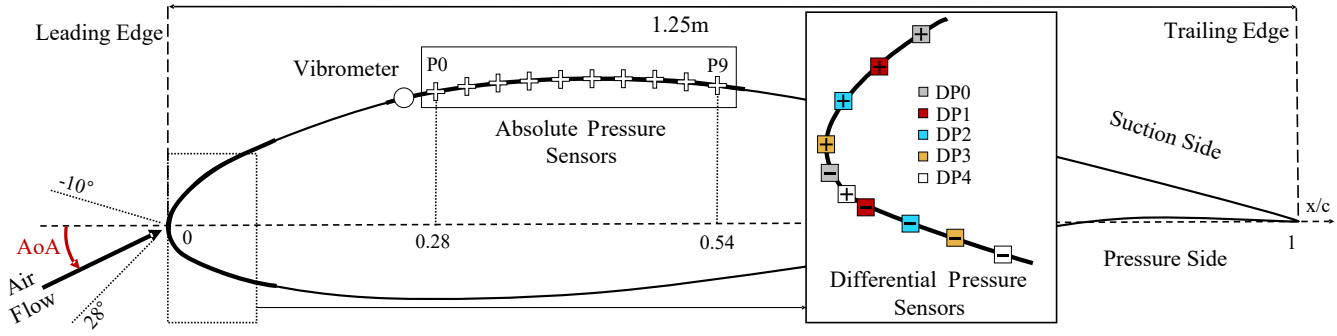

Fig. 1: MEMS sensor distribution on the blade profile. This includes 10 absolute pressure sensors, 5 differential pressure sensors, and one vibrometer. The zoomed-in view of the leading edge shows the arrangement of the positive (+) and negative (-) inlets for the differential pressure sensor. The absolute pressure sensors are located between 24% and 54% of the chord length.

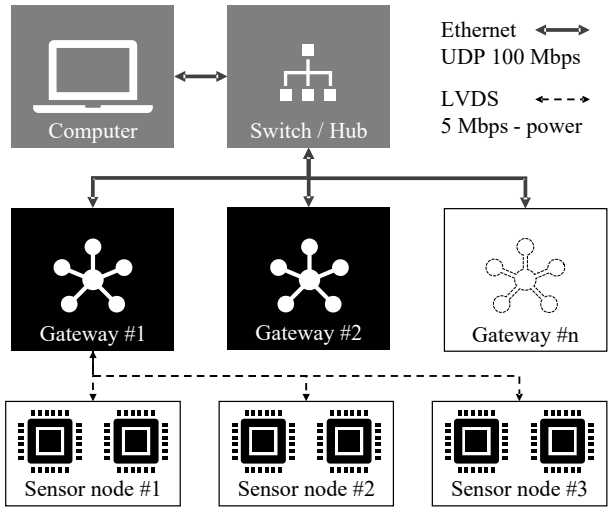

Fig. 2: Acquisition system diagram designed to be modular and support high data rate and thin electronics.

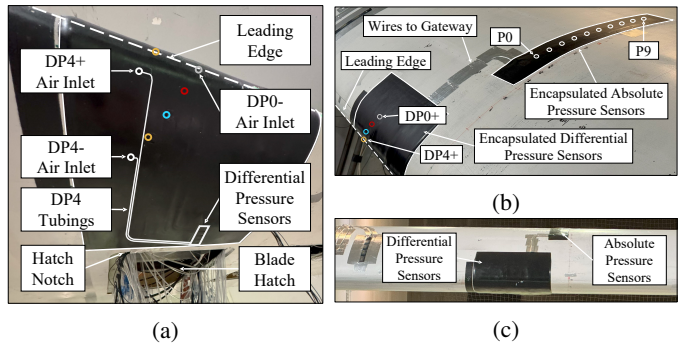

Fig. 3: Photos of the blade in the wind tunnel where sensors presented in Figure 2 are shown in three different angles. Figure 3a is a view of the pressure side, Figure 3b from the suction side, and Figure 3c is a view from the front. In Figure 3a the differential pressure measurement system (inlets, tubings, and sensors) is observable and is highlighted for DP4.

IV. The Modular Acquisition System

The aerodynamic measurement system proposed in this work (Figure 2) must be versatile and modular, supporting heterogeneous setups with concurrent data transfer at different bitrates. Moreover, it must cope with the application scenario described in Section III.

The main constraints were connecting the workstation in the control room to the sensors ($15\,\mathrm{m}$), with a combined throughput above $50\,\mathrm{Mbps}$ and with a total electronic thickness lower than $5\,\mathrm{mm}$ to limit the aerodynamic impact. Many solutions were considered, such as a wireless connection, but the throughput or overhead in power consumption were limiting factors. Therefore, a wired solution was selected. For covering the long distance ($\geq 15\,\mathrm{m}$), we took advantage of the hollowness of the blade to place a gateway that can be accessed through a hatch on the pressure side as seen on Figure 3a. The gateway communicates with the workstation through an Ethernet connection since the thickness is not a concern inside the blade. This connection is used for power and data transfer up to $100\,\mathrm{Mbps}$ exploiting Power over Ethernet (PoE). For the short distance ($\leq 2\,\mathrm{m}$) between the gateway and the sensor boards, flat unshielded cables were chosen. The connectors and cables are $2\,\mathrm{mm}$ and $1\,\mathrm{mm}$ thick respectively, ensuring a low aerodynamic disturbance. For communication, a Universal Asynchronous Receiver Transmitter (UART) bus at $5\,\mathrm{Mbps}$ was used, coupled with Low-Voltage Differential Signaling (LVDS) to amplify the signals from the sensors to the gateway.

The Gateway is a modular board powered via PoE capable of supporting 3 LVDS channels at $5\,\mathrm{Mbps}$ and 10 differential analog input sampled at $16\,\mathrm{kHz}$. It is a compact board built on the dual-core STM32H747, featuring a Cortex-M7 and a Cortex-M4 running at $480\,\mathrm{MHz}$ and $240\,\mathrm{MHz}$ respectively. Its main purpose is interfacing the LVDS serial buses with Ethernet and the UDP protocol. It also enables precise timestamp synchronization. The 3 LVDS channels allow high versatility in supported sensors and provide power up to $2.5\,\mathrm{W}$.

For the scope of this work, two sensor Printed Circuit Boards (PCBs) were designed and deployed on the blade surface. They each feature a maximum thickness of $5\,\mathrm{mm}$ and

an LVDS interface. Each of them uses one of the gateways LVDS channels, as seen in Figure 2. The substrate is a $0.2\,\mathrm{mm}$ Polyimide coupled with a $0.2\,\mathrm{mm}$ stiffener, featuring complete flexibility to perfectly adhere to the blade surface. The two PCBs are based on the STM32L452, and they are manufactured in two different versions. One supports an array of ten absolute pressure sensors and one vibrometer, and the second an array of five differential pressure sensors. Sensor accuracy and sampling rate are detailed in Table I.

The boards are then encapsulated using custom 3D-printed flexible rubber, see Figure 3. This is done to smoothen the surface to limit the impact of the PCB and electronic components on the airflow, which would skew the measurements. It also encapsulates the tubing for the differential pressure sensors.

V. Sensor Selection and Positioning

Building upon the system presented within the Aerosense project [5], [6], a similar set of sensors was selected for the scope of this paper to provide comparable results with previous works. Moreover, the selected sensors should be less than five millimeters thick to not affect the blade aerodynamic performances and with power consumption below $100\,\mathrm{mW}$. Selected commercial MEMS sensors are shown in Table I.

Based on previous research [12], the IIS3DWB high-frequency accelerometer from ST Microelectronics was selected. It is optimized to operate as a vibrometer, acquiring vibration data at a rate up to $26.6\,\mathrm{kHz}$ on 3 axes. It features a power consumption of $3.3\,\mathrm{mW}$ in run mode and a resolution of $0.5\,\mathrm{mg/LSB}$. This paper aims to exploit the vibrometer data to extract other features than blade rotation, such as blade structural health, AoA, resonant frequencies, and flow detachment. The sensor was placed on the upper part of the airfoil at 25% of the chord, at the same distance as the rotation point of the airfoil. More details are present in Figure 1.

The absolute pressure sensors, grouped on a single board with the vibrometer, consist of ten evenly spaced LPS28DFW absolute pressure sensors from ST Microelectronics. The distance between each sensor is the same as the ones from CSTB, i.e., $37\,\mathrm{mm}$, to provide a consistent comparison with the SoA. The sensor is an evolution of the sensor used on Aerosense (LPS27HHW), providing $1.7\times$ better relative accuracy and a power consumption reduction of 28%. The improved relative accuracy eliminates the tedious calibration process previously needed [8]. The sensors were equally distributed on the upper part of the airfoil from 28% to 55% along the chord, where the pressure varies the most when the AoA changes.

The differential pressure board includes five Angst+Pfister 52DL-600BD-491P $60\,\mathrm{mbar}$ differential pressure sensors, featuring a thickness of $5\,\mathrm{mm}$. The sensor nozzles are connected to inlets through plastic tubing. In conjunction with the absolute pressure sensor, they are used to infer the necessary inflow conditions on a rotating blade [14] when located around the leading edge.

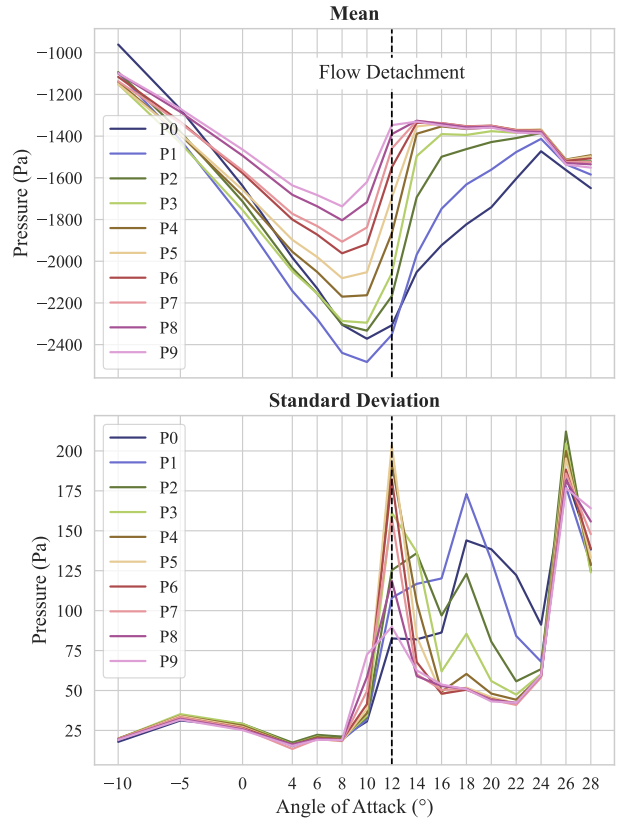

Fig. 4: Mean and standard deviation of the absolute pressure sensors (in Pa) depending on the blade AoA. Measurement relative to the experimental setup in Figure 1.

VI. Experimental Results

The results are presented in terms of mean and standard deviation in Figure 4 for the absolute pressure sensor data, Figure 5 for the differential pressure data, while Figure 6 reports the spectrogram of the vibrometer data. The following experimental analysis shows how each MEMS sensing element selected in Table I can detect the varying aerodynamic response of the blade generated by the AoA sliding. In particular, this paper shows the possibility of inferring the AoA angle, the flow separation occurrence, and spatial position directly from affordable and low-power MEMS sensors, demonstrating how a thin device could be used to estimate the flow conditions around an operative wind turbine blade in real-time.

Following the calibration procedure in [7], [12], the atmospheric pressure measured by the absolute pressure sensor is removed by taking the mean of a 10-second measurement with no wind before each acquisition. The resulting value is then the pressure yielding the aerodynamic force generated by the airfoil, as presented in Figure 4. The aerodynamic force comes mainly from a generated suction on the upper side of the airfoil (hence called the suction side Figure 1), which means the sensors measure negative pressure. When the AoA is increased, the suction increases (i.e., the pressure decreases) linearly with the AoA, an effect clearly visible

TABLE I: Selected MEMS sensors for the experiments reported in Section VI.

Type	Model	Quantity	Sampling Rate [Hz]	Power $[mW]$	R/A Accuracy$^{\diamond}$	Height [mm]	BW [kbps]†
Absolute pressure (barometer)	ST LPS28DFW	10	100	0.95	1.5 Pa / 50 Pa	1.95	24
Differential pressure	Angst+Pfister 52DL	5	1 k	7.26	$\pm 180\,\mu$bar*	5	200
Accelerometer	ST IIS3DWB	1	26.6 k	3.30	0.5 mg$^{\Delta}$	0.86	1200

* Full scale ± 60 mbar, $^{\Delta}$ Full scale ± 16 g, $^{\diamond}$ Relative/Absolute accuracy, † Cumulative generated bitrate

in Figure 4 between $-10°$ and $8°$. This result is confirmed by previous experiments in the same conditions and on the same airfoil [15], where a maximum suction is found at $10°$ before flow separation. Above $10°$, the flow starts to detach on the suction side from the trailing edge, with the separation point moving upstream when the AoA is increased. This effect is visible from the data collected by the array of ten absolute pressure sensors, depicted in Figure 4, where the suction drops down to a local plateau at about -1400 Pa, starting with the pressure sensors closer to the trailing edge. Moreover, the effect of flow separation intrinsically generates increased local fluctuations, which are visible with the rise in standard deviation around $12°$ of Figure 4. Notably, the suction decreases more slowly for the pressure sensors closer to the leading edge, e.g., P0-P3, rather than the ones to the trailing edge side, e.g., P7-P9, between $10°$ and $26°$. For AoA larger than $26°$, the flow becomes truly detached from the airfoil and reaches another state, which is seen by another peak of the standard deviation.

These plots show that it is possible to infer the AoA and the flow separation of an operating wind turbine with low-cost and low-power pressure sensors measuring directly from the blade surface. In total, the ten absolute pressure sensors use 9.5 mW and generate a bandwidth of 24 kbps, while adding an extra-thickness of 1.95 mm, 0.8% of the blade height. From Figure 4, a strict correlation among sensors P0-P9 is visible, thus suggesting an unnecessary redundancy in the measurements. For future optimizations, the system power consumption and cost can be decreased using only a subset of the absolute pressure sensors employed for the scope of this paper.

The five differential pressure sensors measure the pressure difference between two points around the leading edge, marked with $+$ and $-$ in Figure 1. The curvilinear distance between the two measurement points is identical for the five sensors, but these points are slightly shifted between each pair. They are mainly used for a hybrid low-order model inferring the local inflow conditions [14], while the main advantage is the absence of a reference pressure or a zeroing procedure and calibration. The values presented in Figure 5 show that the mean pressure difference for each sensor evolves smoothly with the AoA, with a relatively low standard deviation until complete flow separation when the AoA $>24°$.

Figure 5 shows that it is possible to infer the AoA using only the differential pressure data, which also results in less noise than in Figure 4, thus suggesting an increased measurement precision. However, the flow separation effect is unobservable in this case, happening on the blade suction side. In total, the

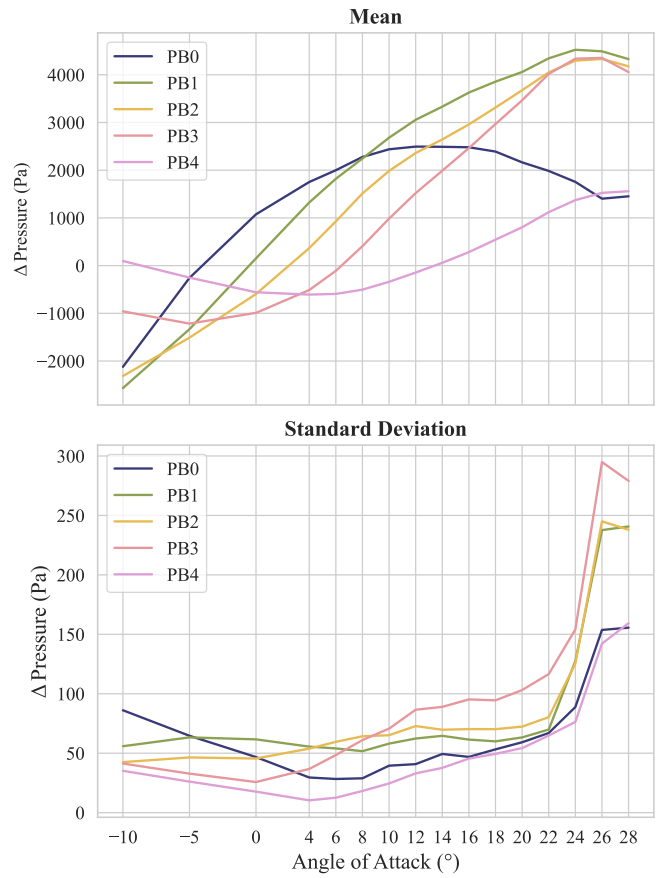

Fig. 5: Mean and standard deviation of the differential pressure sensors (in Pa) depending on the blade AoA. Measurement relative to the experimental setup in Figure 1.

five differential pressure sensors use 36.3 mW and generate a bandwidth of 200 kbps, while adding an extra-thickness of 5 mm, 2% of the blade height. From Figure 5, a strict correlation between sensors PB1-PB3 is visible, suggesting an unnecessary redundancy in the measurements. For future optimizations, the system power consumption and cost can be decreased using only a subset of the differential pressure sensors.

Results in Figure 4 and Figure 5 have shown how the flow separation is associated with relevant fluctuations, which may be further detected from the vibration data from the vibrometer, specifically in the frequency domain. Figure 6 depicts the vibrometer spectrogram, calculated for each AoA. A focus was made on frequencies between 0 and 60 Hz, where the majority ($>90\%$) of the signal energy is present, in which

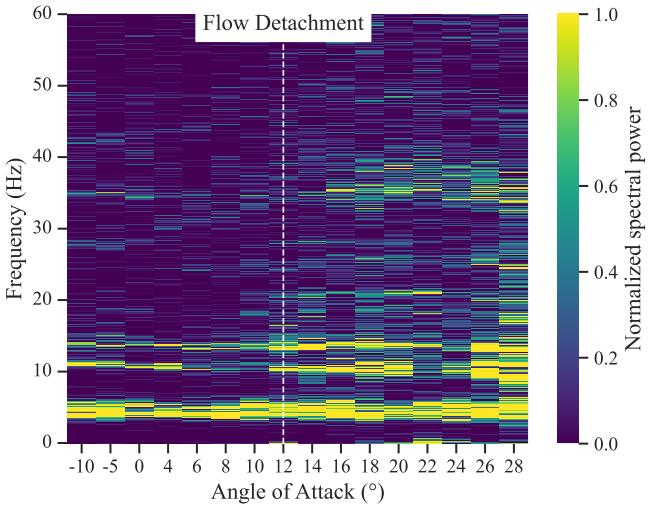

Fig. 6: Spectrogram of the vibrometer data relative to the AoA. Measurement relative to the experimental setup in Figure 1.

4 main components of the modal frequency are observed. A trend related to the AoA sliding is visible. The lower component is constant around $5\,\mathrm{Hz}$, which defines the main structural modal component. The second and third ones are respectively around 11 and $13\,\mathrm{Hz}$, with an increased standard deviation above an AoA of $12°$. The fourth modal component evolves from 27 to $35\,\mathrm{Hz}$. These latter two demonstrate a trend related to the AoA and the flow detachment. Notably, the signal energy between 20 and $60\,\mathrm{Hz}$ below $12°$ is negligible. However, above $12°$, when the flow detachment happens consistently with Figure 4, high-frequency components start to appear, which evolve proportionally with the AoA. In this case, the flow fluctuations generated by the flow detachment cause structural oscillations visible with the vibrometer.

The differential pressure sensors needs $3.3\,\mathrm{mW}$ and generates a bandwidth of $1.2\,\mathrm{Mbps}$, while adding an extra-thickness of $0.86\,\mathrm{mm}$, 0.3% of the blade height. The high amount of data this sensor generates could be a problem for low-power MCUs, such as the one in the Aerosense system. However, since the main modal components are located below $60\,\mathrm{Hz}$, the sensor-generated data can be drastically decreased, reducing the sampling rate $10\times$.

VII. Conclusion

Monitoring wind flow and operational parameters of wind turbines directly in the field is a fundamental prerequisite for optimizing sustainable electrical generation efficiency. The aerodynamics of the rotating blades is of particular interest; however, many technical and scientific challenges still exist due to the complexity of measurement system installations on the edge. This paper demonstrates how a heterogeneous set of thin and low-power MEMS sensors can be installed directly on the surface of a 1:1 scale blade, acquiring key aerodynamic and operative parameters, such as AoA and flow detachment. Experimental results in a wind tunnel show a precision of $1°$ with a total sensing power below $50\,\mathrm{mW}$. Basic summary statistics (i.e., means and standard deviation) are enough for inferring key parameters about the AoA and flow detachment on the pressure sensors. For the vibrometer, frequency analysis can help infer those features. Moreover, the proposed modular acquisition system supports a future study to optimize the number and the type of sensors needed to extract aerodynamic parameters.

References

[1] A. K. Kanál and K. Tamás, "Assessment of indoor air quality of educational facilities using an IoT solution for a healthy learning environment," in *2020 IEEE International Instrumentation and Measurement Technology Conference (I2MTC)*. IEEE, 2020, pp. 1–6.

[2] G. Artale, A. Cataliotti, G. Caravello, V. Cosentino, S. Guaiana, D. Di Cara, N. Panzavecchia, G. Tinè, V. Antonucci, M. Ferraro *et al.*, "A monitoring and management system for energy storage integration in smart grids," in *2019 IEEE International Instrumentation and Measurement Technology Conference (I2MTC)*. IEEE, 2019, pp. 1–6.

[3] M. Fahim, V. Sharma, T.-V. Cao, B. Canberk, and T. Q. Duong, "Machine learning-based digital twin for predictive modeling in wind turbines," *IEEE Access*, vol. 10, pp. 14 184–14 194, 2022.

[4] S. Wang, C. Wang, H. Ding, Z. Chen, and J. Ye, "Influence of operation conditions on condensation and aerodynamic shockwave in supersonic nozzle," in *2022 IEEE International Instrumentation and Measurement Technology Conference (I2MTC)*. IEEE, 2022, pp. 1–6.

[5] R. Fischer, H. Mueller, T. Polonelli, L. Benini, and M. Magno, "Windnode: A long-lasting and long-range bluetooth wireless sensor node for pressure and acoustic monitoring on wind turbines," in *2021 4th IEEE International Conference on Industrial Cyber-Physical Systems (ICPS)*. IEEE, 2021, pp. 393–399.

[6] T. Polonelli, H. Müller, W. Kong, R. Fischer, L. Benini, and M. Magno, "Aerosense: a self-sustainable and long-range bluetooth wireless sensor node for aerodynamic and aeroacoustic monitoring on wind turbines," *IEEE Sensors Journal*, vol. 23, no. 1, pp. 715–723, 2022.

[7] J. Deparday, H. Müller, T. Polonelli, and S. Barber, "An experimental system to acquire aeroacoustic properties on wind turbine blades," in *Journal of Physics: Conference Series*, vol. 2265, no. 2. IOP Publishing, 2022, p. 022089.

[8] T. Polonelli, J. Deparday, H. Müller, R. Fischer, L. Benini, S. Barber, and M. Magno, "Aerosense: Long-range bluetooth wireless sensor node for aerodynamic monitoring on wind turbine blades," in *Journal of Physics: Conference Series*, vol. 2265, no. 2. IOP Publishing, 2022, p. 022074.

[9] F. Zonzini, M. M. Malatesta, D. Bogomolov, N. Testoni, A. Marzani, and L. De Marchi, "Vibration-based SHM with upscalable and low-cost sensor networks," *IEEE Transactions on Instrumentation and Measurement*, vol. 69, no. 10, pp. 7990–7998, 2020.

[10] F. P. G. Márquez and A. M. P. Chacón, "A review of non-destructive testing on wind turbines blades," *Renewable Energy*, vol. 161, pp. 998–1010, 2020.

[11] K. Brinker, A. Case, and M. T. Al Qaseer, "Bistatic microwave sensor for in-situ composite inspection and structural health monitoring," in *2021 IEEE International Instrumentation and Measurement Technology Conference (I2MTC)*. IEEE, 2021, pp. 1–6.

[12] P. Trummer, T. Polonelli, J. Deparday, I. Abdallah, and M. Magno, "Blade position and motion estimation on the surface of a rotating wind turbine through a single MEMS IMU," in *2023 9th International Workshop on Advances in Sensors and Interfaces (IWASI)*. IEEE, 2023, pp. 40–45.

[13] I. Neunaber, F. Danbon, A. Soulier, D. Voisin, E. Guilmineau, P. Delpech, S. Courtine, C. Taymans, and C. Braud, "Wind tunnel study on natural instability of the normal force on a full-scale wind turbine blade section at reynolds number 4.7 · 106," *Wind Energy*, vol. 25, no. 8, pp. 1332–1342, 2022.

[14] Y. Marykovskiy, J. Deparday, I. Abdallah, G. Duthé, S. Barber, and E. Chatzi, "Hybrid model for inflow conditions inference on airfoils under uncertainty," *AIAA Journal*, vol. 61, no. 11, pp. 4913–4925, 2023.

[15] C. Braud, B. Podvin, and J. Deparday, "Study of the wall pressure variations on the stall inception of a thick cambered profile at high reynolds number," 2023.